MODE GROWTH AN COMPETITION IN THE X-RAY FREE ELECTRON LASER OSCILLATOR START-UP FROM NOISE*

R.R. Lindberg† and K.-J. Kim, ANL, Argonne, IL 60439, USA

Abstract

We describe the radiation properties of an x-ray free electron laser oscillator, beginning with its start-up from noise through saturation. We decompose the initially chaotic undulator radiation into the longitudinal modes of the resonator whose properties are largely determined by the transverse gain profile and the bandwidth of the Bragg mirror. Because the radiation is initially comprised of several modes whose growth rates are comparable, we show that only after many oscillator passes is the output pulse dominantly characterized by the lowest-order, gaussian mode. Understanding the full longitudinal structure during the initial amplification will be critical in assessing the tolerances on the electron beam, undulator, and optical cavity required for robust operation.

INTRODUCTION

The basic principles of a free electron laser (FEL) oscillator are well-known (see, e.g., [1]), involving the successive FEL gain of radiation confined in an optical cavity. Recently, such an FEL design was proposed for x-rays [2], in which the electron beam has a low emittance ~ 0.1 mm $\cdot$ mrad, and the resonator cavity is created using Bragg mirrors that have high reflectivities for x-rays over very narrow bandwidths [3]. Typically, the per pass linear FEL gain $g \sim 0.3$, while the total power losses in an optimized cavity can be as low as $\alpha \sim 0.1 - 0.25$. Such a device is predicted to provide Fourier-limited, picosecond x-ray pulses of MW power at repetition rates ~ 1 MHz, thereby serving as a complementary source to those based on self-amplified spontaneous emission, such as LCLS [4].

In this paper we derive the supermode equation describing the linear growth and longitudinal profile of the radiation. We then show how these modes are initially seeded by the chaotic undulator radiation, resulting in the competition between various longitudinal modes. We conclude with some results obtained for possible 5, 12, and 20 keV radiation sources based on a FEL oscillator driven by a 7 GeV high-brightness electron beam.

LINEAR SUPERMODE THEORY

In this section we derive the growing modes of the x-ray FEL oscillator, i.e., the cavity supermodes. Supermode analysis of FELs was introduced in Ref. [5]; our work follows the simplified approach developed by Elleaume [6].

* Work supported by U.S. Dept. of Energy, Office of Basic Energy Sciences, Contract No. DE-AC02-06CH11357.
† lindberg@aps.anl.gov

For the case of x-rays, the coherence length σ_c of the undulator radiation is much less than the inverse bandwidth of the Bragg mirror (typically $\lambda/\sigma_c \sim 1/N_u \sim 10^{-3}$ while $\sigma_\omega \lambda \sim 10^{-5} - 10^{-6}$), so that slippage can be safely ignored. The radiation evolution during any pass can then be approximately described as a succession of FEL gain, followed by reflection from the narrow-band Bragg mirrors, followed by a displacement in distance from the next electron bunch. Assuming a peak linear gain of g, a gaussian electron beam of width σ_e, a reflection transfer function $R(\omega)$, and a radiation-bunch displacement of ℓ, the radiation evolution can be depicted by the following three steps:

$$\text{gain} : |E(\tau)|^2 \rightarrow \left[1 + g\, e^{-\tau^2/2\sigma_e^2}\right] |E(\tau)|^2 \quad (1)$$

$$\text{mirror} : E(\tau) \rightarrow \int d\omega\; e^{i\omega\tau} R(\omega) E(\omega) \quad (2)$$

$$\text{displacement} : E(\tau) \rightarrow E(\tau + \ell), \quad (3)$$

where $\tau \equiv z - ct$ is the co-moving bunch coordinate. To simplify the problem further, we make several approximations. First, we assume that the linear gain g is small and real, and expand the beam profile about its maximum. Next we assume that the Bragg mirror reflection function is gaussian $R(\omega) \approx (1-\alpha/2)e^{-\omega^2/\sigma_\omega^2}$, with α the loss and σ_ω the single mirror spectral bandwidth, and furthermore assume that in the frequency region of large reflectivity (i.e., where lasing occurs) $R(\omega)$ can be Taylor expanded to lowest order in ω. Finally, we assume that ℓ is sufficiently small to make a Taylor expansion here as well. Under these assumptions, the relations (1)-(3) are simplified to:

$$\text{gain} : E(\tau) \rightarrow \left(1 + \frac{g}{2} - \frac{g\tau^2}{4\sigma_e^2}\right) E(\tau) \quad (4)$$

$$\text{mirror} : E(\tau) \rightarrow \left(1 - \frac{\alpha}{2} + \frac{1}{\sigma_\omega^2}\frac{\partial^2}{\partial\tau^2}\right) E(\tau) \quad (5)$$

$$\text{displacement} : E(\tau) \rightarrow \left(1 + \ell\frac{\partial}{\partial\tau}\right) E(\tau). \quad (6)$$

We now use the simplified equations (4)-(6) to relate the longitudinal E field starting pass number $n+1$ to that at the beginning of pass n. Assuming that the per pass change is small, so that $E_{n+1} - E_n \approx \frac{\partial}{\partial n} E$, we find that the evolution is described by the following partial differential equation:

$$\frac{\partial}{\partial n} E(\tau, n) = \left[\frac{1}{\sigma_\omega^2}\frac{\partial^2}{\partial\tau^2} - \frac{g\tau^2}{4\sigma_e^2} + \frac{1}{2}(g - \alpha) + \ell\frac{\partial}{\partial\tau}\right] E(\tau, n). \quad (7)$$

We note that the first line of this equation can be directly related to the quantum mechanical simple harmonic oscillator. Thus, it comes as little surprise that the solution to

(7) is given in terms of the Gauss-Hermite functions:

$$E_m(\tau,n) = e^{n\Lambda_m} e^{-\tau\sigma_\omega^2\ell/2} \times \exp\left[\frac{\sqrt{g}\sigma_\omega}{2\sigma_e}\tau^2\right] H_m\left[g^{1/4}\sqrt{\frac{\sigma_\omega}{\sigma_e}}\tau\right], \quad (8)$$

where $\Lambda_m \equiv \frac{1}{2}[(g-\alpha) - \sigma_\omega^2\ell^2/2 - \sqrt{g}(2m+1)/\sigma_e\sigma_\omega]$ is the per pass amplitude gain and H_m is the Hermite polynomial of order m. From this, we deduce that in order to avoid significant gain reduction we must first demand the electron bunch-radiation timing errors to be much less than the inverse crystal bandwidth, typically $\ell \lesssim 0.2/\sigma_\omega$. To avoid unnecessary complications, we assume perfect timing for the remainder of the paper, so that $\ell = 0$. Additionally, modes of higher order have less gain, and all modes suffer significant gain reduction when $\sigma_e\sigma_\omega \lesssim 1$; thus, we require the electron bunch length to be greater than the inverse crystal bandwidth $\sigma_e \gtrsim 1/\sigma_\omega$ to insure sufficient per pass gain for lasing.

An example of supermode evolution is shown in Fig. 1, for which the parameters correspond to 5 keV radiation from the high-brightness, 7 GeV beam shown in Table 1. These results were obtained using a 1-dimensional FEL simulation code derived by integrating the transverse electron orbits over their unperturbed trajectories, and by assuming that the transverse radiation profile is a gaussian mode whose Rayleigh range Z_R is dictated by the cavity geometry. This model includes the lowest-order effects of energy spread, transverse beam emittance, and radiation diffraction, and has demonstrated remarkable agreement with the single slice results of both the 2-dimensional code GINGER and the 3-dimensional code GENESIS. The electron β_z-function and radiation Z_R is chosen by maximizing the FEL gain; typically $\beta_z \approx Z_R \approx L_u/2\pi$ [7]. We decompose the longitudinal radiation profile into the Gauss-Hermite mode functions in Fig. 1, in which the growth of the three lowest order modes can be clearly seen, with a growth rate decreasing as the mode order m increases. Additionally, we can identify three distinct regions of mode evolution, roughly delineated in Fig. 1 as regions (a), (b), and (c). Region (a) is dominated by the spontaneous undulator radiation that provides an initially chaotic seeding for the various modes. After the fluctuations have grown to a sufficient level, the exponential growth characteristic of linear gain can be seen in region (b). During this phase of evolution, we see that the modes each grow with their characteristic growth rate that decreases as the mode order number m increases. Finally, when the radiation amplitude is sufficient to decrease the gain, we arrive at the nonlinear saturation region (c). While the $m = 0$ and $m = 1$ mode smoothly level, we also see additional growth of the $m = 2$ mode. Inspection of the longitudinal profile of the saturated radiation indicates that this corresponds to a broadening of the cavity pulse, as the optical pulse width becomes comparable to that of the electron beam σ_e. In the following sections we further elaborate on the physics of the supermode growth, from the initially chaotic seeding though saturation.

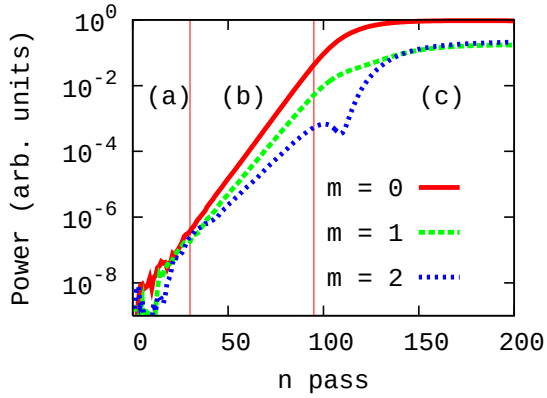

Figure 1: Example of supermode growth for the lowest three order modes. The evolution of the modes can be roughly divided into three regions: region (a) gives the initial chaotic seeding from the spontaneous undulator radiation; region (b) depicts the linear growth of the supermodes, with the gaussian $m = 0$ mode having the largest growth; region (c) is characterized by nonlinear saturation of the gain, where the growth of higher order symmetric modes (like the $m = 2$) reflects pulse broadening as it approaches the electron bunch length.

INITIAL SEEDING FROM NOISE

We model the chaotic spontaneous radiation as a random collection of gaussian spikes, each of whose width is the undulator coherence length $\sigma_c \sim N_u\lambda$:

$$E(\tau) = \sum_j \mathcal{E}_0 \exp\left[-\frac{(\tau-\tau_j)^2}{2\sigma_c^2} - \frac{\tau^2}{2\sigma_e^2}\right] \quad (9)$$

$$\Rightarrow E(\omega) \approx \sum_j \sqrt{2\pi}\sigma_c\mathcal{E}_0 \exp\left[-\frac{\sigma_c^2}{2}\omega^2 - i\omega\tau_j - \frac{\tau_j^2}{2\sigma_e^2}\right]$$

where j indexes the bunch electrons, and the radiation envelope is modulated by the electron bunch length $\sigma_e \gg \sigma_c$. The Bragg crystal effectively filters the radiation in frequency space as given by (2), where we approximate $R(\omega)$ as a lossy gaussian filter with width $\sigma_\omega \ll 1/\sigma_c$ and power loss α. Thus, after reflection and filtering by the two Bragg mirrors, the electric field can be approximately written as

$$E(\tau) \approx \sum_j \left(1-\tfrac{\alpha}{2}\right)\sigma_c\sigma_\omega\mathcal{E}_0 \times \exp\left[-\sigma_\omega^2(\tau-\tau_j)^2 - \frac{\tau^2}{2\sigma_e^2}\right]. \quad (10)$$

Comparing (9) and (10), we see that over after one pass the characteristic amplitude of the spontaneous undulator radiation is decreased by $(1-\alpha/2)\sigma_c\sigma_\omega$: the finite reflectivity of the crystal contributes the factor $(1-\alpha/2) \sim 1$, while the reduction by $\sigma_c\sigma_\omega \ll 1$ arises because the bandpass of the crystal is much narrower than the characteristic bandwidth of the undulator radiation. Furthermore, the narrow bandwidth of the crystal serves to stretch the spikes of the spontaneous radiation, transforming them into random oscillations whose characteristic frequency $\omega \sim \sigma_\omega$.

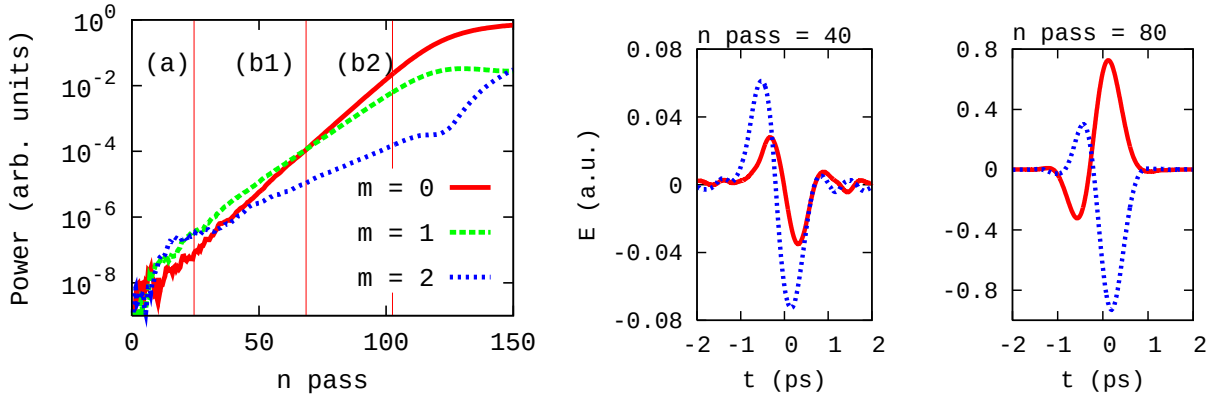

Figure 2: Example where the initial random seeding is largest in the $m = 1$ mode, using the same parameters (but different seeding) as in Fig. 1. The first plot shows initial seeding of first order mode in region (a), after which the linear growth phase is dominated by the $m = 1$ mode through region (b1). Due to its larger growth rate, the component of the $m = 0$ mode eventually becomes dominant in region (b2). We show examples of the real (red solid line) and imaginary (blue dotted line) parts of the scaled electric field after 40 passes and after 80 passes. While there is still a significant antisymmetric part after 80 passes, it becomes a diminishing component, and at saturation the pulse is nearly gaussian.

To determine how the initially chaotic spontaneous undulator radiation overlaps with the supermodes of the x-ray FEL oscillator, we first decompose a single frequency oscillation into the supermode (i.e., Gauss-Hermite) basis:

$$E(\tau) = \mathscr{A}\cos(\omega\tau) + \mathscr{B}\sin(\omega\tau) = \sum_m C_m \frac{e^{-\tau^2/2\mathrm{w}^2}}{\sqrt{2^m m!\sqrt{\pi}}} H_m(\tau/\mathrm{w}),$$

where the mode coefficients are C_m and the width of the supermode is defined via $\mathrm{w}^2 = \sqrt{g}\,\sigma_\omega/\sigma_e$. To determine the overlap of the supermodes with the chaotic radiation, we use the orthogonality of the Gauss-Hermite functions. While the mode coefficients can be written analytically in terms of Hermite polynomials, we will focus here on the two lowest order modes, for which we find

$$C_0 = \mathscr{A}\frac{\sigma_e\sqrt{2\sqrt{\pi}}}{\sqrt{\sigma_e^2+\mathrm{w}^2}}\exp\left[-\frac{\sigma_2^2\mathrm{w}^2}{\sigma_e^2+\mathrm{w}^2}\omega^2\right] \quad (11)$$

$$C_1 = \mathscr{B}\frac{\sigma_e^3\mathrm{w}\sqrt{\sqrt{\pi}}}{(\sigma_e^2+\mathrm{w}^2)^{3/2}}\,\omega\exp\left[-\frac{\sigma_2^2\mathrm{w}^2}{\sigma_e^2+\mathrm{w}^2}\omega^2\right]. \quad (12)$$

Expressions (11)-(12) describe the overlap of the supermode with any single frequency component. Since the filtered undulator radiation is comprised of a continuum of frequencies, the relevant mode overlap is obtained by averaging C_m over the spectrum distribution. We recall that the characteristic frequency of the oscillations is σ_ω, and introduce the (approximate) averaging operator $\langle\cdot\rangle$ via:

$$\big\langle\mathscr{X}(\omega)\big\rangle \equiv \sqrt{\tfrac{2}{\pi\sigma_\omega^2}}\int_0^\infty d\omega\; e^{-\omega^2/2\sigma_\omega^2}\;\mathscr{X}(\omega). \quad (13)$$

The general expression of the averaged mode coefficients is rather cumbersome, involving the Gauss function. However, two important limits are easily obtained:

$$\mathrm{w}^2 \gg 1/\sigma_\omega^2: \quad \big\langle C_0\big\rangle \approx \frac{\sqrt{\pi}\mathscr{A}}{2\mathscr{B}}\big\langle C_1\big\rangle \quad (14)$$

$$\mathrm{w}^2 \sim 1/\sigma_\omega^2: \quad \big\langle C_0\big\rangle \gg \frac{\mathscr{A}}{\mathscr{B}}\big\langle C_1\big\rangle \quad (15)$$

The second limit implies that mode width (and, hence, σ_e) is of order the inverse crystal bandwidth $1/\sigma_\omega$, so that the filtered spontaneous radiation only has significant overlap with the lowest order gaussian mode. While this can provide a single, Fourier-limited longitudinal peak, as mentioned in the previous section the concomitant decrease in effective mode gain can prevent effective lasing of the oscillator. In the first limit (14), on the other hand, the mode width is significantly shorter than the electron beam, and overlap of the spontaneous radiation typically has similar components in the two lowest order modes (since $\mathscr{A} \sim \mathscr{B}$).

We consider the limit $\mathrm{w}^2 \gg \sigma_e^2$ a bit further, since this yields the highest gain and is often satisfied in practice (as in Fig. 1). Furthermore, as indicated in (14), the seeding of the two lowest order modes tends to be comparable. We can obtain further insight by calculating the fluctuation of the average mode, $\big\langle C_{0,1}^2\big\rangle$. Again, while the specifics are a bit complicated, it is straightforward to show that

$$\mathrm{w}^2 \gg 1/\sigma_\omega^2: \quad \frac{\big\langle C_{0,1}^2\big\rangle^{1/2}}{\big|\big\langle C_{0,1}\big\rangle\big|} \sim \big(\mathrm{w}\,\sigma_\omega\big)^{1/2} > 1, \quad (16)$$

namely, that the mode coefficients are typified by large fluctuations about their mean. This can result in significant seeding of higher order modes in such a way that the pulse is no longer largely Gaussian in linear gain regime [i.e., region (b) of Fig. 1]. We show an example of this phenomenon in Fig. 2. The first graph demonstrates that the initial fluctuating phase [region (a)] can sometimes dominantly seed the first order mode. The linear growth phase is

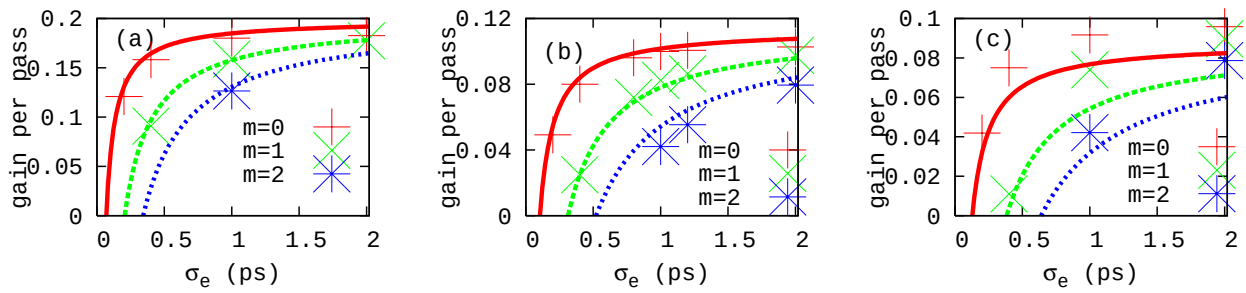

Figure 3: Supermode gain rates for the 5keV (a), 12 keV (b), and 20 keV (c) radiation cases detailed in Table 1, using a per pass cavity loss $\alpha = 0.25$. Simulation points were determined by decomposing the longitudinal radiation onto the Gauss-Hermite modes, and are plotted for the lowest three order modes when they could be determined (and are non-zero). Theory is given by the lines, where the power growth rate $2\Lambda_m \equiv [(g-\alpha) - \sigma_\omega^2 \ell^2/2 - \sqrt{g}(2m+1)/\sigma_e\sigma_\omega]$, and we have replaced $g \to (1-\alpha)g$ so that Λ_0 reduces to the infinite pulse per pass gain of $[(1+g)(1-\alpha)-1]$.

then initially dominated by the antisymmetric $m = 1$ mode through region (b1). As the amplification continues, however, the radiation approaches a gaussian due to the higher growth rate of the $m = 0$, so that it becomes the dominant component throughout region (b2).

We also show two examples of complex electric field envelopes in the linear gain region in Fig. 2. After 40 passes we see that both the real (red solid lines) and imaginary (blue dotted lines) parts of E are largely described by the $m = 1$ supermode; after 80 passes the pulse has more overlap with the $m = 0$ mode, although there is still a significant antisymmetric component from the mode with $m = 1$. As evolution continues the pulse becomes more symmetric, until it is nearly gaussian at saturation.

EXAMPLES FOR A 7 GEV BEAM

In this section we present supermode evolution results relevant to a low-emittance, 7 GeV electron beam whose current is 10 A. We detail the electron beam and undulator parameters in Table 1, in which we also include the saturated cavity power predicted by the 1-dimensional simulation discussed previously, and the saturated cavity power obtained from 2-dimensional GINGER simulations for comparison. We assume a normalized crystal bandpass $\sigma_\omega/\omega = 3.4 \times 10^{-6}$, and a total per pass cavity loss $\alpha = 0.15$; in the 12 keV case this could arise from 6% loss from the mirrors (including 4% loss from the radiation out-coupling) and an additional 5% loss per pass for each of two focusing elements.

We show the measured and theoretical per pass gain for the modes $m = 0,\ 1,\ 2$ as a function of the electron bunch length σ_e in fig. 3 for the 5 keV (a), 12 keV (b), and 20 keV (c) radiation. In each scenario the per pass gain decreases as the bunch length decreases, until reaching zero gain for $\sigma_e \sim 1/\sigma_\omega$. Since the gain decreases more rapidly for the higher order modes, the cavity pulse becomes more gaussian as the electron bunch length decreases.

Table 1: Possible undulator and beam parameters for three different radiation wavelengths produced by a 7 GeV beam with $I_{\rm peak} = 10$ Amp and $\Delta\gamma/\gamma = 0.02\%$. The saturated power $P_{\rm sat}$ given by our 1D code and the 2D code GINGER were determined assuming mirror losses $\alpha = 0.15\%$.

Parameter	**5 keV**	**12 keV**	**20 keV**
λ_u (cm)	2.24	1.76	1.50
N_u	1000	3000	3000
K	2.50	1.51	1.05
β_x (m)	5.0	9.0	10.0
ϵ_x (m·rad)	2×10^{-7}	2×10^{-7}	10^{-7}
g	0.42	0.28	0.32
$P_{\rm sat}$ (1D)	120 MW	23 MW	25 MW
$P_{\rm sat}$ (2D)	90 MW	25 MW	16 MW

CONCLUSIONS

We have shown that the linear supermodes of the x-ray FEL oscillator are the growing Gauss-Hermite modes. Seeding of these modes by the chaotic undulator radiation seeds is random, so that the initial evolution may be dominated by higher-order longitudonal modes. Nevertheless, the lowest order $m = 0$ gaussian mode eventually dominates due to its larger growth rate, so that the final longitudinal radiation profile is nearly gaussian at saturation.

REFERENCES

[1] C. Brau, *Free-Electron Lasers* (Academic Press, 1990).

[2] K.-J. Kim, Y. Shvyd'ko, and S. Reiche, Phys. Rev. Lett. **100**, 244802 (2008).

[3] Y. Shvyd'ko, *X-Ray Optics - High Energy-Resolution Applications*, (Springer, 2004).

[4] LCLS Conceptual Design Report, SLAC-R-593 (2002).

[5] G. Dattoli, A. Marino, A. Renieri, and F. Romanelli, IEEE J. Quant. Elect. **QE-17** 1371 (1985).

[6] P. Elleaume, IEEE J. Quant. Elect. **QE-17** 1012 (1981).

[7] K.-J. Kim, Nucl. Instr. Meth. Res. A. **A318**, 489 (1992).